

## Contents

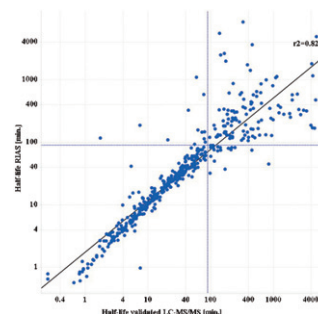
### Regular articles

1–9

#### An integrated platform for fully automated high-throughput LC–MS/MS analysis of *in vitro* metabolic stability assay samples

Andreas H. Luippold, Thomas Arnhold, Wolfgang Jörg, Roderich D. Süßmuth

A new system was setup and validated for the high-throughput LC–MS/MS analysis of metabolic stability samples in a real-life application with a speed of 8s/sample (see figure for correlation validated LC–MS/MS system ( $x$ -axis) to new system ( $y$ -axis)).

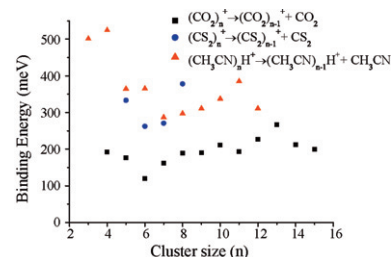


10–14

#### Measurements of kinetic energy release and binding energy following the unimolecular fragmentation of molecular cluster ions

R. Parajuli, B.J. Duncombe, A.J. Stace

Cluster binding energies from unimolecular decay.

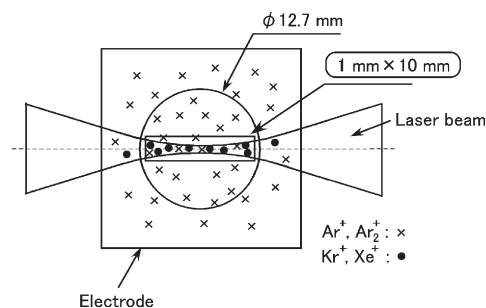


15–20

#### Improvement of the resonance ionization mass spectrometer performance for precise isotope analysis of krypton and xenon at the ppt level in argon

Yoshihiro Iwata, Chikara Ito, Hideki Harano, Takafumi Aoyama

An electrode with a slit was applied to limit the  $\text{Ar}^+$  and  $\text{Ar}_2^+$  ions reaching the detector without loss of the  $\text{Kr}^+$  and  $\text{Xe}^+$  ion signals.

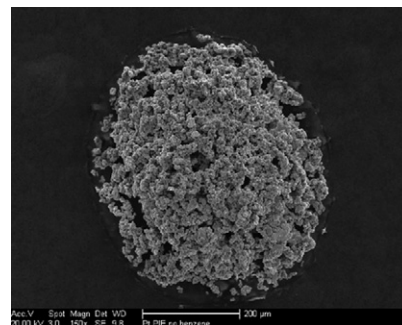


## 21–24

**Porous ion emitters—A new type of thermal ion emitter**

Matthew G. Watrous, James E. Delmore, Mark L. Stone

The porous ion emitter is sintered onto the center of a conventional thermal ionization filament and an aqueous solution containing the sample wicked into this emitter.

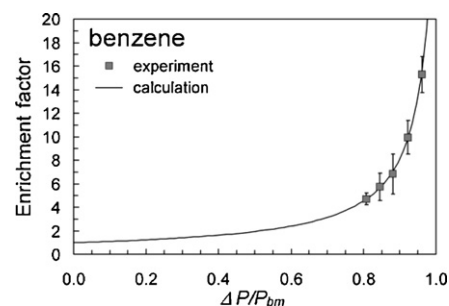


## 25–29

**Membrane introduction system for trace analysis of volatile organic compounds using a single photon ionization time-of-flight mass spectrometer**

Yukio Yamamoto, Nozomu Kanno, Kenichi Tonokura, Akihiro Yabushita, Masahiro Kawasaki

► A silicone membrane sample introduction system combined with a vacuum ultraviolet single photon ionization time-of-flight mass spectrometer has been developed to detect trace volatile organic compounds.

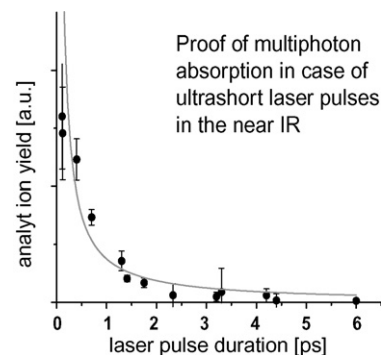


## 30–35

**Chirp dependent matrix-assisted laser desorption/ionization measurements of alkali metal adapted angiotensin II by using ultrashort laser pulses in the near IR regime**

J.M. Wichmann, F. Schwaneberg, C. Lupulescu, A. Lindinger

► Pulse feature dependence of the MALDI-signal. ► Multiphoton absorption in the MALDI-Process. ► Cationization process of angiotensin II during MALDI.

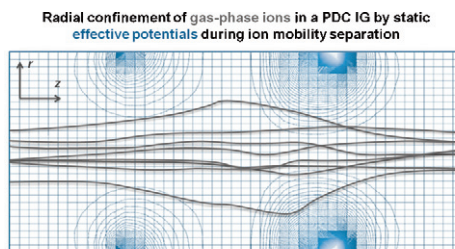


## 36–42

**Gas-phase ion dynamics in a periodic-focusing DC ion guide**

Joshua A. Silveira, Chaminda M. Gamage, Ryan C. Blase, David H. Russell

► The PDC IG is an ion mobility spectrometer that yields high ion transmission via suppression of radial diffusion. ► Ions are confined in the radial dimension by effective potentials which are present at the electrode edges. ► The axial electric field, assisted by collisional cooling, dampens ion kinetic energy near the back edge of electrodes to allow effective potentials to direct ion motion.

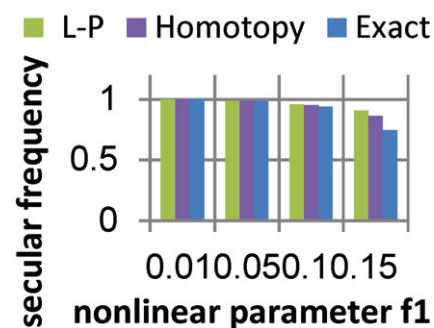


## 43–46

### Comparison of calculated axial secular frequencies in nonlinear ion trap by homotopy method with the exact results and the results of Lindstedt–Poincaré approximation

Alireza Doroudi

► The secular frequencies of a nonlinear ion trap are calculated. ► Only hexapole superposition are considered as nonlinearity. ► Homotopy perturbation method is used. ► The results are compared with the results of Lindstedt–Poincaré method and the exact results.

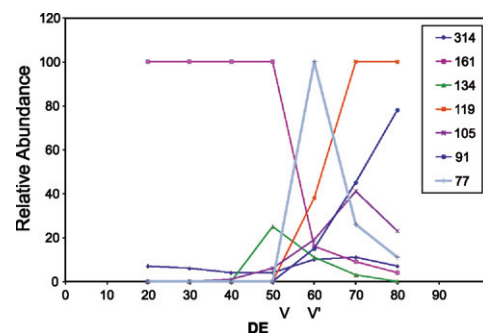


## 47–52

### Effect of dissociation energy: Signal to noise ratio on ion formation and sensitivity of analytical method for quantification and confirmation of triazofos in blood samples using gas chromatography–mass spectrometer (GC–MS/MS)

Sukesh Narayan Sinha

► GC–MS method was developed for qualify and quantify of triazofos in blood sample. ► This method gives combined picture of confirmation and quantification of triazofos. ► The correlation between ion formation and dissociation energy were demonstrated. ► The LOD and LOQ was 0.351 and 1.17 ngmL<sup>-1</sup> respectively with 99% accuracy. ► The new ion was isolated at  $m/z$  161 (100%), with 83.9 to 111% recovery on 50V DE.

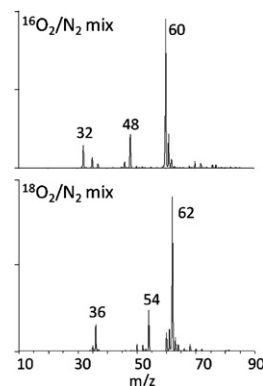


## 53–58

### Production and utilization of CO<sub>3</sub><sup>-</sup> produced by a corona discharge in air for atmospheric pressure chemical ionization

Robert G. Ewing, Melanie J. Waltman

► CO<sub>3</sub><sup>-</sup> is the most prevalent anion produced in a point-to-plane corona discharge in air. ► The identity of CO<sub>3</sub><sup>-</sup> was confirmed using <sup>18</sup>O<sub>2</sub> and was likely generated from the interactions between O<sub>3</sub><sup>-</sup> and CO<sub>2</sub>. ► Nitroglycerine forms an adduct with CO<sub>3</sub><sup>-</sup>. ► The fragmentation of this adduct yields CO<sub>3</sub><sup>-</sup> and not NO<sub>3</sub><sup>-</sup> indicating a relatively high electron affinity of CO<sub>3</sub><sup>-</sup>.



## 59–64

### Ion kinetic energy measurements in two soft ion ejection methods from a quadrupole ion trap

Maria A. van Agthoven, Philippe Colomby, Michel Surugue, Claude Beaugrand, Franck L. Wind, Jean-Claude Tabet

► Ions are ejected at higher RF voltages than expected along the  $\beta_z = 0$  line. ► Ion ejection efficiency increases with DC voltages on the ion trap. ► Ion kinetic energy increases with DC voltage at ejection. ► Ion kinetic energy increases with RF voltage amplitude at ejection.

